Supporting Information

Polyaniline-Encapsulated NiFe Layered Double Hydroxide Electrocatalyst for Robust Water Oxidation

Fengming Zhang,[a] Filip Ublekov,[b] Yue Li,[a] Wenbo Zhao,[a] Shucheng Liu,[a] Fangming Liu,[ae] Jinhan Li,[a] Meng Yu,*[a] and Fangyi Cheng*[acd]

a Key Laboratory of Advanced Energy Materials Chemistry (Ministry of Education), Engineering Research Center of High-efficiency Energy Storage (Ministry of Education), Frontiers Science Center for New Organic Matter (Ministry of Education), College of Chemistry, Nankai University, Tianjin 300071, China.
E-mail: nkyu2023@nankai.edu.cn, fycheng@nankai.edu.cn.

b Institute of Polymers, Bulgarian Academy of Sciences, 1113 Sofia, Bulgaria.

c Haihe Laboratory of Sustainable Chemical Transformations, Tianjin 300192, China.

d Liaoning Binhai Laboratory, Dalian 116000, China.

e Nankeyouyi (Tianjin) Technology Co., Ltd. Tianjin 300192, China.

*Corresponding authors.

1 Experimental

1.1 Materials and Reagents

$NaNO_3$ (99%), $Ni(NO_3)_2 \cdot 6H_2O$ (98%), and $FeSO_4 \cdot 7H_2O$ (99.95% metals basis) were purchased from Aladdin (Shanghai, China). Aniline (99.5%) was obtained from Macklin (Shanghai, China). In this work, nickel foam (NF, Sinero (Suzhou, Jiangsu, China)) with a thickness of 0.5 mm is used as a conductive substrate. All the above reagents were used as received unless otherwise noted.

1.2 Material characterizations

The morphology and element distribution of materials were characterized using scanning electron microscopy (SEM, JSM-7900F) and high-resolution transmission electron microscopy (HRTEM, Talos F200X G2), equipped with energy-dispersive X-ray spectroscopy (EDS) and selected area electron diffraction (SAED). Powder X-ray diffraction spectra (XRD) were recorded on a SmartLab 9 kW diffractometer with Cu-Kα radiation. X-ray photoelectron spectroscopy (XPS) was performed with an Axis Ultra DLD. Raman spectra were collected using a confocal Raman microscope (Renishaw inVia-Qontor Raman Microscope) with an excitation wavelength of 532 nm and a 50× objective. Elemental analysis was conducted using inductively coupled plasma-optical emission spectroscopy (ICP-OES, SpectroBlue). The Ni K-edge and Fe K-edge X-ray absorption near-edge spectroscopy (XANES) and extended X-ray absorption fine structure (EXAFS) data of catalysts were collected using bench-top easyXAFS300+ instrument (easyXAFS, LLC) with a Si551 spherically bent crystal analyzer and silver anode X-ray tube. The data analysis of XANES and EXAFS was conducted utilizing the ATHENA and ARTEMIS modules (version 0.9.26) within the IFEFFIT software suite.[1]

1.3 Synthesis of electrocatalysts

1.3.1 Synthesis of PANI/NiFe LDH

The PANI/NiFe LDH was fabricated on NF by a two−step electrodeposition method. Before the electrodeposition, the NF (1.0 cm × 2.0 cm × 0.5 mm) was treated with deionized water, ethanol, and 1.0 M HCl successively, and then rinsed with deionized water to remove surface impurities and oxide layers. The electrodeposition was carried out in a two-electrode system at room temperature. NF and graphite rod were respectively used as the working and counter electrode. In the first electrodeposition process,

the electrolyte was composed of 0.03 M $Ni(NO_3)_2$, 0.01 M $FeSO_4$, and 0.1 M $NaNO_3$. The cathodic electrodeposition was carried out at −5 mA·cm^{-2} for 2 minutes to obtain NiFe LDH/NF. After being washed with deionized water, the as-prepared NiFe LDH/NF was placed in the electrolyte containing 0.1 M $NaNO_3$ and 0.05 M aniline for anodic electrodeposition. The second electrodeposition was performed at 10 mA·cm^{-2} for 30 seconds to obtain PANI/NiFe LDH/NF. The final product was rinsed and dried at 60 °C in a vacuum oven.

1.3.2 Synthesis of other electrocatalysts

The preparation of NiFe LDH and PANI was similar to PANI/NiFe LDH/NF with one-step electrodeposition. The PANI/NiFe LDH/CC and NiFe LDH/CC were prepared similarly to PANI/NiFe LDH and NiFe LDH, except that the carbon cloth (CC) served as the working electrode. In the synthesis of the Pt/C electrode, 7.5 mg 20% Pt/C, 75 μL Nafion D-521 dispersion, and 1.5 mL isopropyl alcohol were mixed into a uniform ink under ultrasonic conditions. The ink was sprayed on carbon paper (CP) and dried under vacuum at 50 °C. The load mass of Pt/C on CP is approximately 1.6 mg·cm^{-2}.

1.4 Electrochemical measurements

The electrochemical tests were carried out on an Ivium-n-stat electrochemical workstation under ambient temperature conditions. The as-prepared electrode, Hg/HgO electrode, and Pt foil were employed as working, reference, and counter electrodes. The cyclic voltammetry (CV) and linear sweep voltammetry (LSV) curves were collected in 1.0 M KOH aqueous solution with 95% iR-compensation. Electrochemical impedance spectroscopy (EIS) measurements were performed at 1.50 V vs. RHE, with frequencies ranging from 100 kHz to 0.1 Hz and an amplitude of 10 mV. The chronopotentiometry (CP) curves were collected in 1.0 M KOH under 500 mA·cm^{-2}. All these measured potentials were converted to values relative to the reversible hydrogen electrode (RHE) using the following equation:

$$E_{vs.\,RHE} = E_{vs.\,Hg/HgO} + E^{\ominus}_{Hg/HgO} + 0.059pH$$

The electrochemical active surface area (ECSA) of each catalyst was estimated from the double layer capacitance (C_{dl}) in a potential window where no faradaic currents are involved (0.1-0.2 V vs. Hg/HgO), which is determined by performing CV scans at the scan rate of 40-140 mV·s^{-1}. The C_{dl} is obtained as half

the slope of a plot that shows the difference between anodic and cathodic current density at 0.15 V vs. Hg/HgO against the scan rate. The ECSA was calculated according to the following equation:

$$ECSA = \frac{C_{dl}}{C_s}$$

where C_s is 40 μF·cm^{-2}.

The turnover frequency (TOF) values of PANI/NiFe LDH and NiFe LDH were calculated according to the following equation:[2]

$$TOF = \frac{J \times A}{4 \times F \times m}$$

where J is the current density at a given potential, A is the geometric area of the electrode, F is the Faraday constant (96485 C mol^{-1}) and m is the amount of reactive sites determined as the total number of Ni and Fe atoms from the ICP-OES results in this work.

1.5 Assembly of the anion exchange membrane water electrolysis device

The anion exchange membrane water electrolysis (AEM) device is composed of anode (PANI/NiFe LDH/NF or NiFe LDH/NF electrode, 2.0 cm × 2.0 cm × 0.5 mm), cathode (Pt/C electrode, 2.0 cm × 2.0 cm × 0.2 mm), anion exchange membrane (AEM, AM01-50, 3.5 cm × 3.5 cm × 50 μm, KMem Tech, China), gas diffusion layer (GDL, NF, 2.0 cm × 2.0 cm × 0.5 mm), gaskets and end plate with flow fields. The 1.0 M KOH solution was used as an electrolyte introduced into both the anode and cathode sides. LSV curves of the devices were measured from 1.0 to 3.0 V_{cell} at a scan rate of 10 mV·s^{-1}.

1.6 In situ electrochemical Raman measurements

For in situ Raman measurements, a confocal Raman microscope (Renishaw inVia-Qontor Raman Microscope) with an excitation wavelength of 532 nm and a spectro-electrochemical cell was adopted. The Raman spectra of the catalysts were collected with the as-prepared catalysts, Pt wire, and saturated Ag/AgCl serving as working, counter, and reference electrode, respectively.

2 Results and discussion

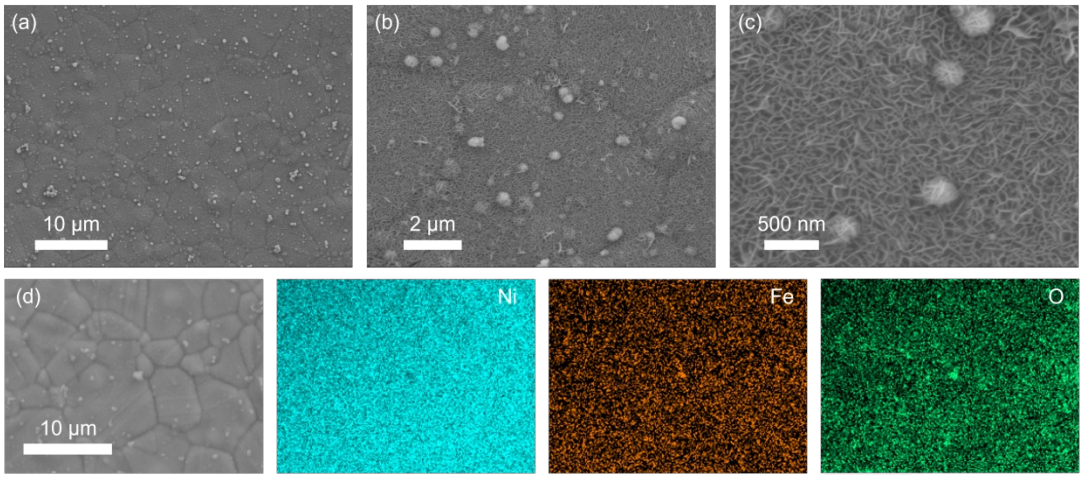

Fig. S1. (a-c) The SEM images of NiFe LDH under different magnifications and (d) the related EDS mappings of Ni, Fe, and O elements.

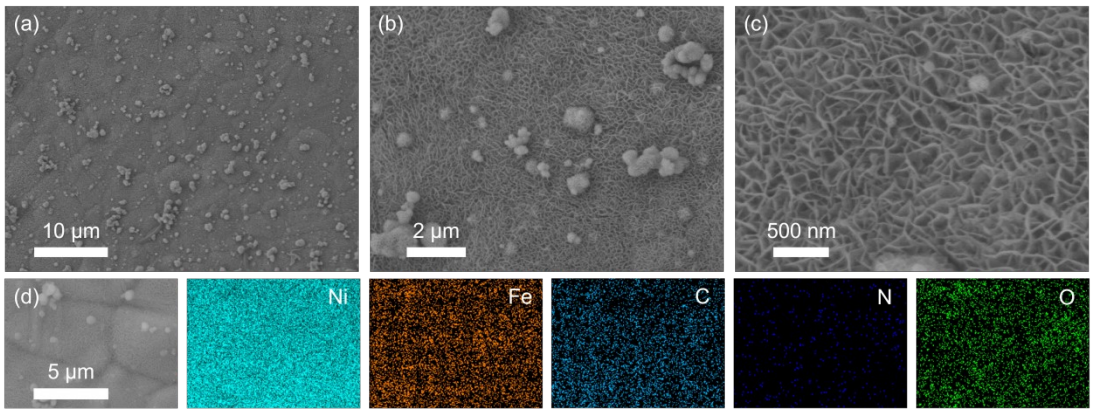

Fig. S2. (a-c) The SEM images of PANI/NiFe LDH under different magnifications and (d) the related EDS mappings of Ni, Fe, C, N, and O elements.

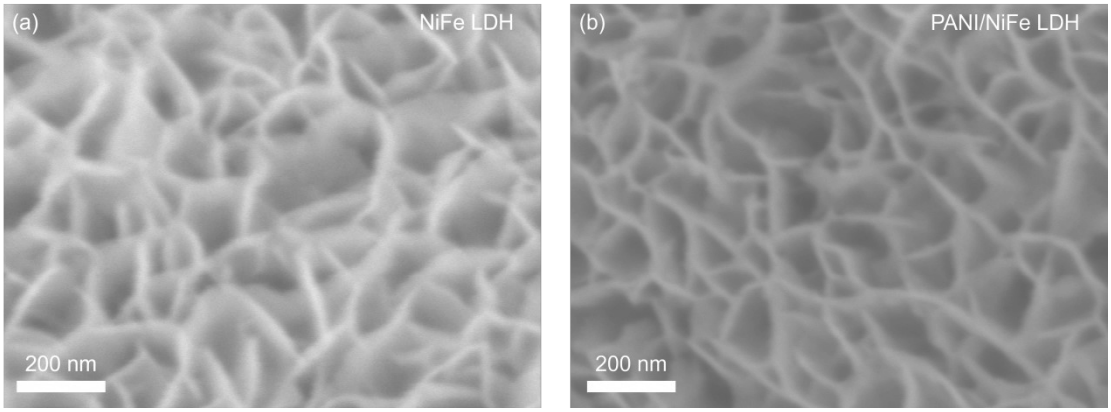

Fig. S3. The SEM images of (a) NiFe LDH and (b) PANI/NiFe LDH under higher magnification.

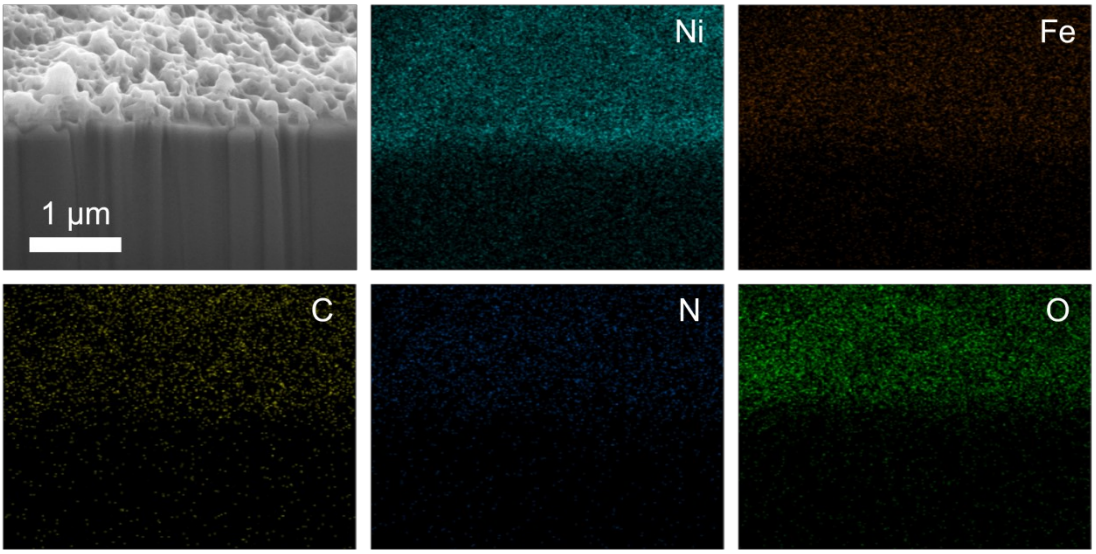

Fig. S4. The cross-sectional EDS mappings of PANI/NiFe LDH.

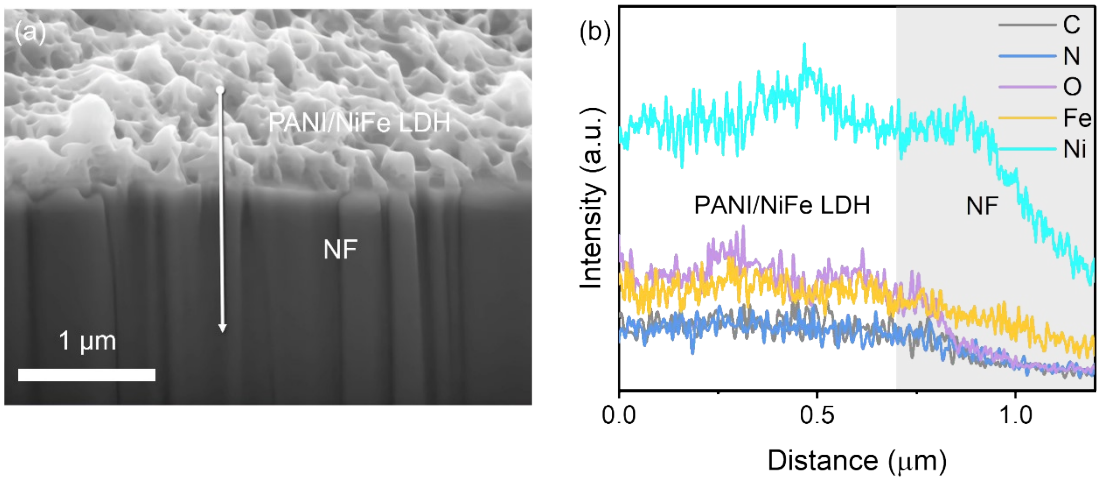

Fig. S5. The cross-sectional EDS linear scan of PANI/NiFe LDH following the white arrow in Fig. S5a.

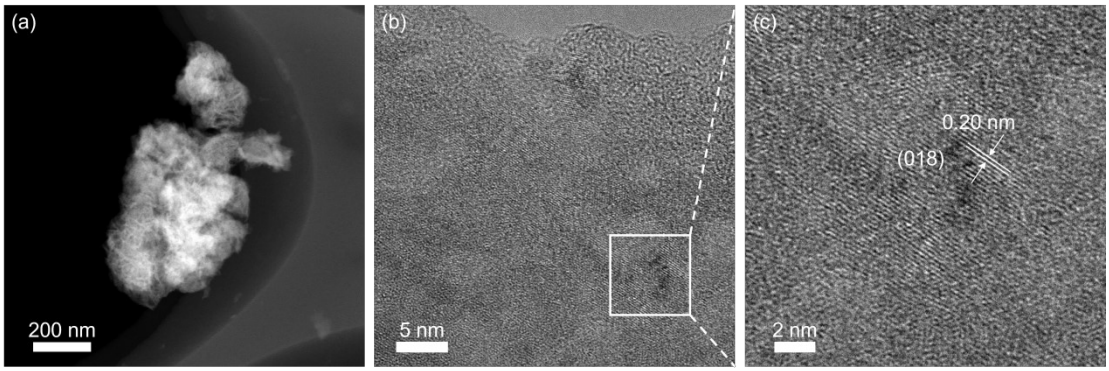

Fig. S6. (a) The TEM image and (b,c) HRTEM images of NiFe LDH.

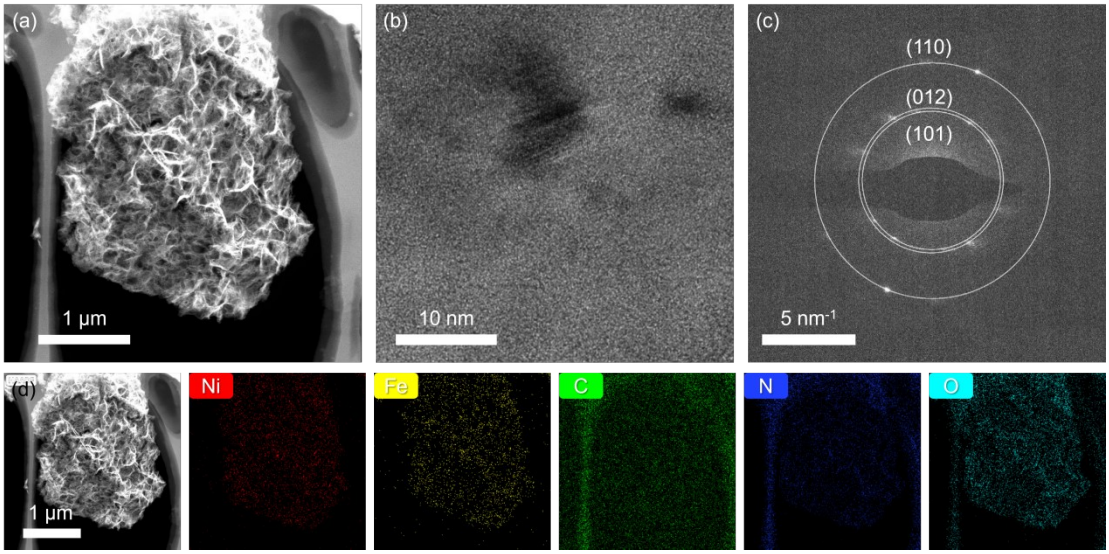

Fig. S7. (a) The TEM image, (b) HRTEM image, and (c) SAED pattern of PANI/NiFe LDH. (d) The corresponding EDS mappings of PANI/NiFe LDH.

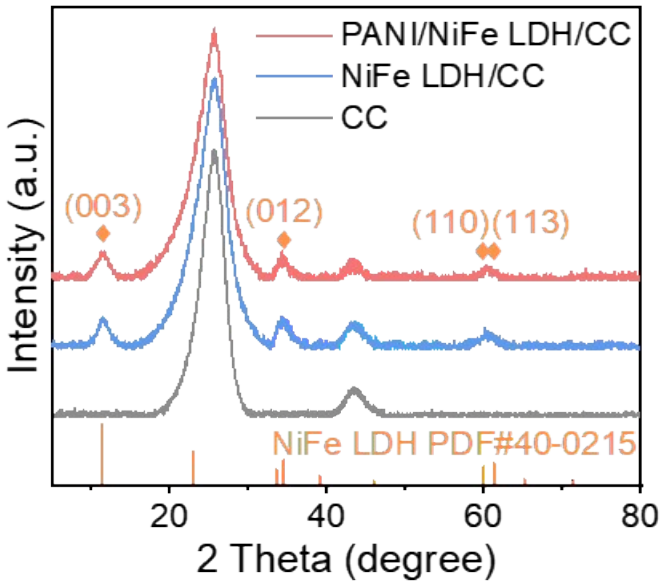

Fig. S8. XRD patterns of PANI/NiFe LDH and NiFe LDH on carbon cloth (CC).

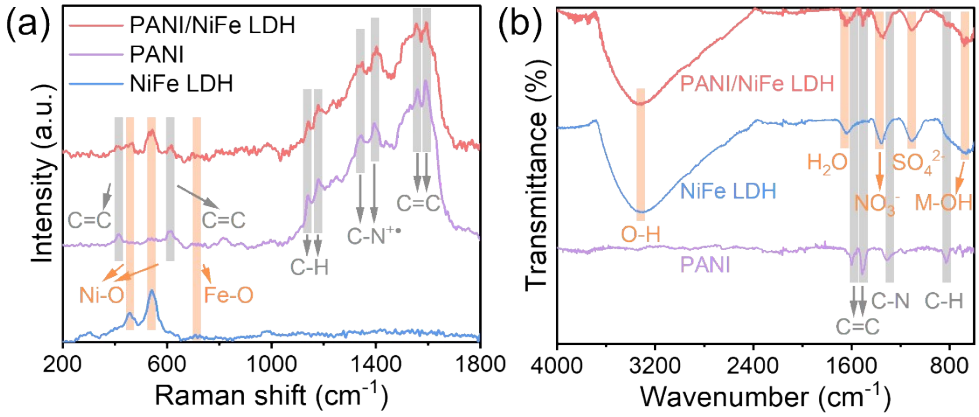

Fig. S9. (a) Raman and (b) FT-IR spectra of PANI/NiFe LDH, PANI, and NiFe LDH.

In the Raman spectra of NiFe LDH and PANI/NiFe LDH, peaks at 459 cm^{-1}, 542 cm^{-1}, and 711 cm^{-1} were ascribed to the Ni-O and Fe-O vibrations in NiFe LDH.[3] In the spectra of PANI and PANI/NiFe LDH, peaks at 1140 cm^{-1} , 1182 cm^{-1} (C-H), 1345 cm^{-1} , 1395 cm^{-1} ($C-N^{+\cdot}$), 1562 cm^{-1} and 1591 cm^{-1} (C=C) corresponded to PANI.[4-6] FTIR spectra of NiFe LDH and PANI/NiFe LDH showed signals at 3310 cm^{-1} (O-H), 1634 cm^{-1} (H_2O), and 656 cm^{-1} (M-OH), attributed to NiFe LDH.[7] Meanwhile, peaks at 1350 cm^{-1} and 1106 cm^{-1} corresponded to NO_3^- and SO_4^{2-} that introduced in the synthesis process,[8, 9] respectively. In the FTIR spectra of PANI and PANI/NiFe LDH, peaks at 1596 cm^{-1} (C=C) and 1516 cm^{-1} (C=C), 1317 cm^{-1} (C-N), and 833 cm^{-1} (C-H) corresponded to PANI.[4]

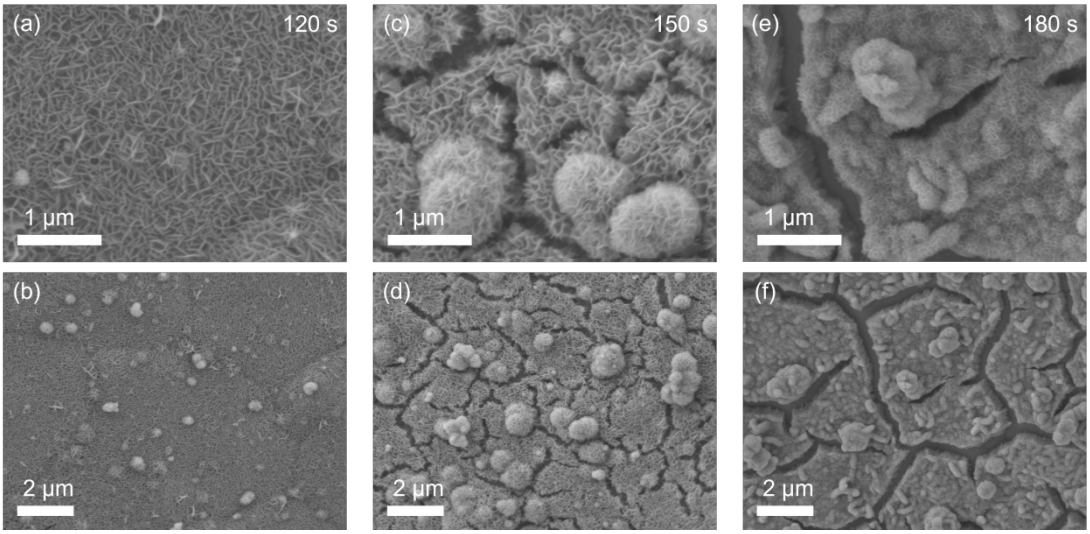

Fig. S10. The SEM images of NiFe LDH prepared with various deposition times under different magnifications.

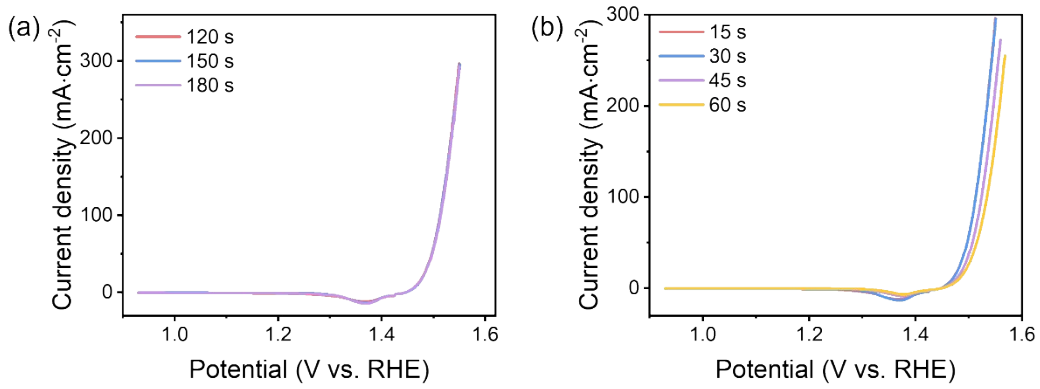

Fig. S11. (a) LSV curves of NiFe LDH with different deposition times. (b) LSV curves of PANI/NiFe LDH with different deposition times of PANI.

The deposition parameters for PANI/NiFe LDH were subsequently optimized by preparing catalysts with different deposition times. SEM images of NiFe LDH synthesized with varying deposition times indicated that a duration of 120 s produced a nanosheet structure without significant cracks (Fig. S8). Further increase in deposition time of NiFe LDH led to gradual formation of cracks on the surface of the electrode owing to mechanical stress, which negatively impacted the operational stability of NiFe LDH, significantly accelerating structural degradation during OER. Linear sweep voltammetry (LSV) curves of NiFe LDH with different deposition times revealed that the prolonged deposition time primarily affected the extent of cracking, while no significant change in the OER catalytic activity (Fig. S9a). LSV curves of PANI/NiFe LDH prepared with varying PANI deposition times indicated minimal differences in electrochemical performance at 30 s or less (Fig. S9b). However, increasing the deposition time to 45 s significantly decreased the catalytic activity of PANI/NiFe LDH, suggesting that a thicker coating of PANI may block the catalytic active site on NiFe LDH. Therefore, deposition times of 120 and 30 s were optimal for the NiFe LDH and PANI deposition, respectively.

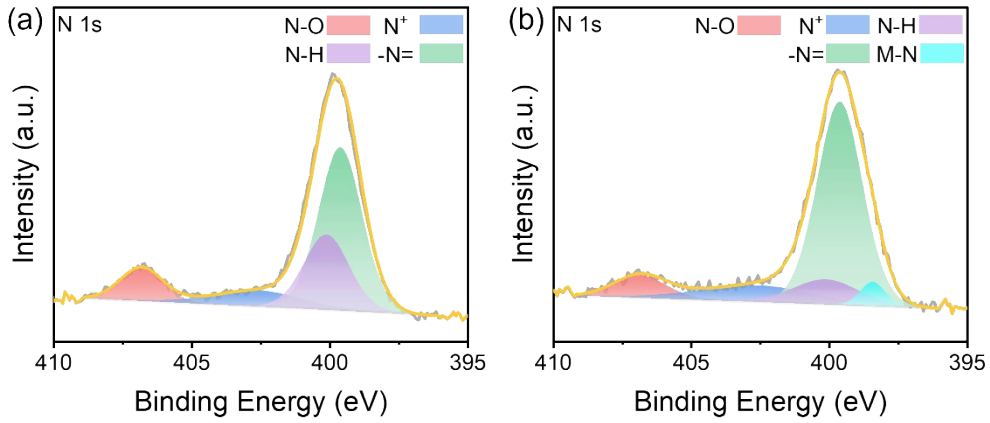

Fig. S12. The high-resolution N 1s XPS spectrum of (a) PANI and (b) PANI/NiFe LDH.

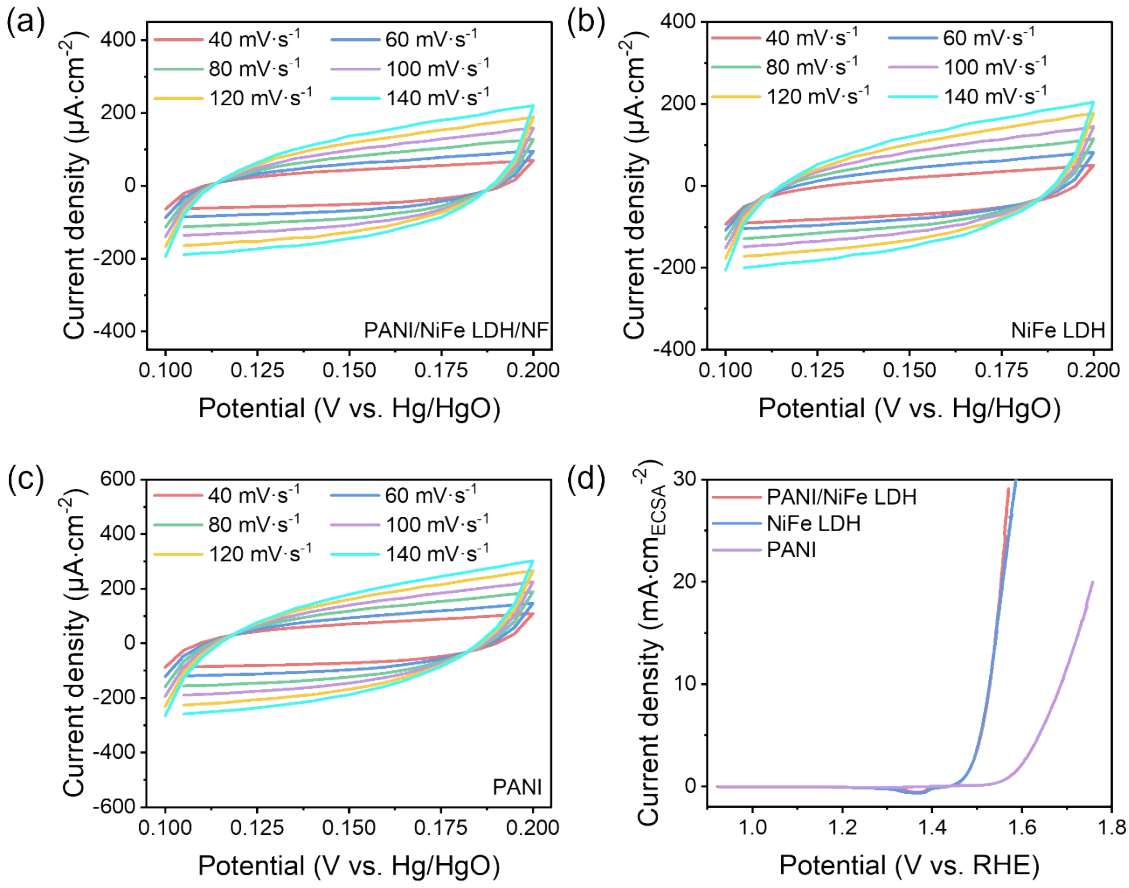

Fig. S13. The CV curves of (a) PANI/NiFe LDH, (b) NiFe LDH, and (c) PANI in the non-polarized region at different scan rates. (d) LSV curves normalized by the ECSA of PANI/NiFe LDH, NiFe LDH and PANI.

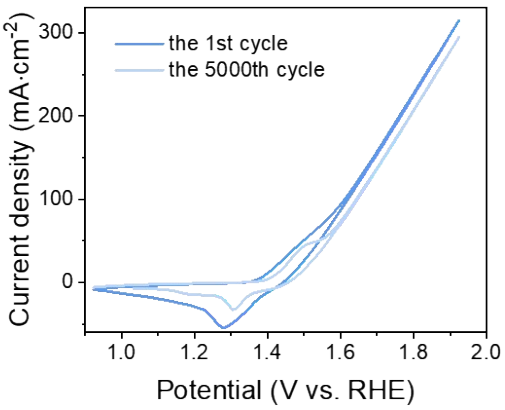

Fig. S14. The accelerated duration test of NiFe LDH performed with a scan rate of 50 mV·s^{-1}.

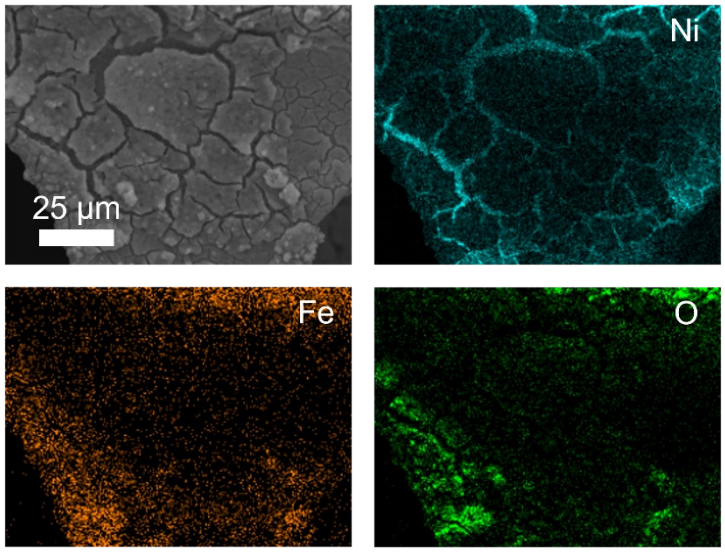

Fig. S15. The EDS mappings of NiFe LDH after the 500 h chronopotentiometry test.

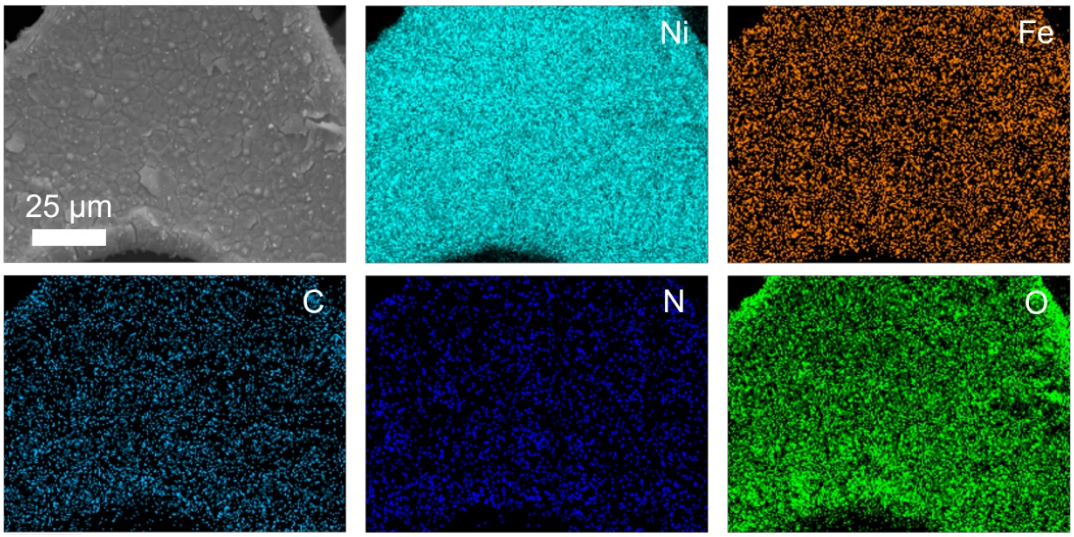

Fig. S16. The EDS mappings of PANI/NiFe LDH after the 500 h chronopotentiometry test.

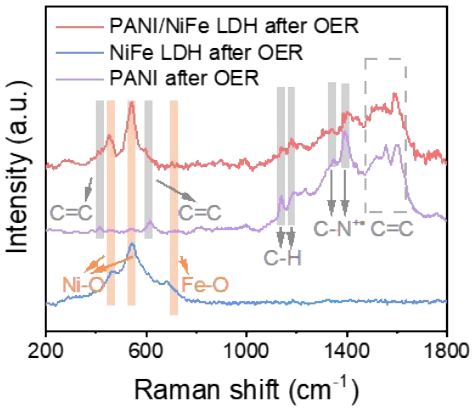

Fig. S17. Raman spectra of PANI/NiFe LDH, PANI and NiFe LDH after 10 h chronopotentiometry test.

After the 10-hour CP test, the characteristic peaks observed at 1140 cm^{-1}, 1180 cm^{-1}(C-H), 1347 cm^{-1}, 1390 cm^{-1} (C-$N^{+\cdot}$), 1557 cm^{-1} and 1599 cm^{-1} (C=C) in PANI/NiFe LDH are attributed to PANI, indicating that PANI remains stable and undergoes no significant change during the OER process.

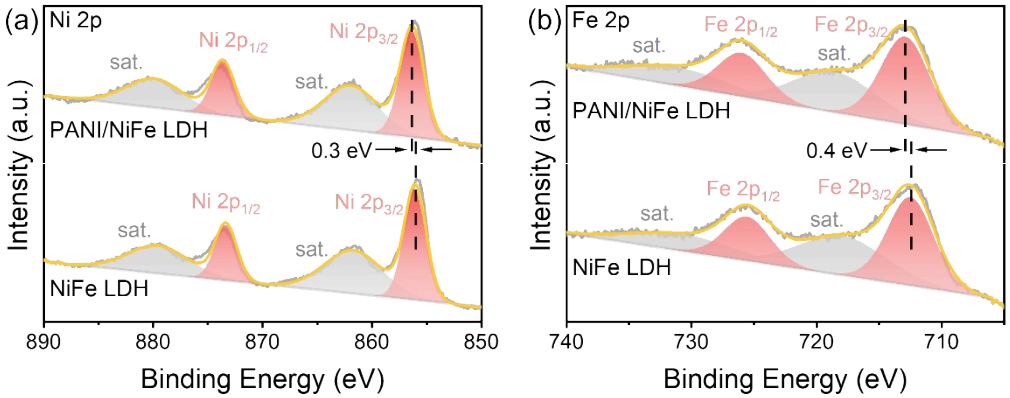

Fig. S18. The high-resolution (a) Ni 2p and (b) Fe 2p XPS spectra of PANI/NiFe LDH and NiFe LDH after a 10-hour CP test at 500 $mA \cdot cm^{-2}$.

According to the post-reaction XPS analysis, both PANI/NiFe LDH and NiFe LDH underwent oxidation, increasing in the metal oxidation states. For PANI/NiFe LDH, the Ni 2p3/2 and Fe 2p3/2 shift from 855.9 to 856.3 eV and 712.4 to 712.8 eV, respectively. Moreover, both Ni and Fe in PANI/NiFe LDH showed higher binding energy compared to NiFe LDH (856.0 eV and 712.4 eV). This indicated that PANI stabilizes the high-valent metal centers through coordination to enhance the operational stability.

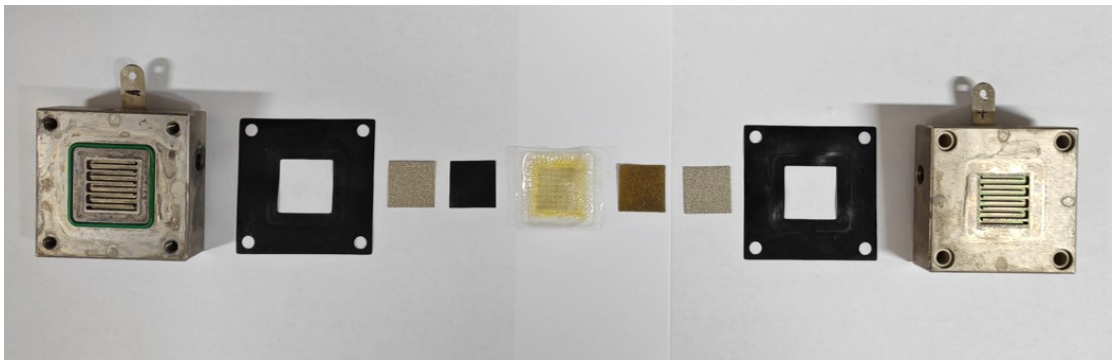

Fig. S19. The Optimal image of the AEMWE device.

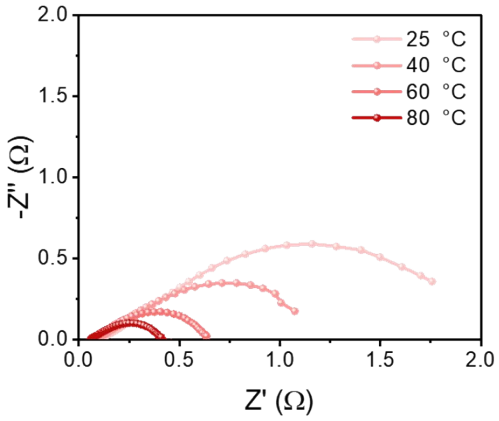

Fig. S20. The EIS Nyquist plots of PANI/NiFe LDH-based AEMWE device under different temperatures.

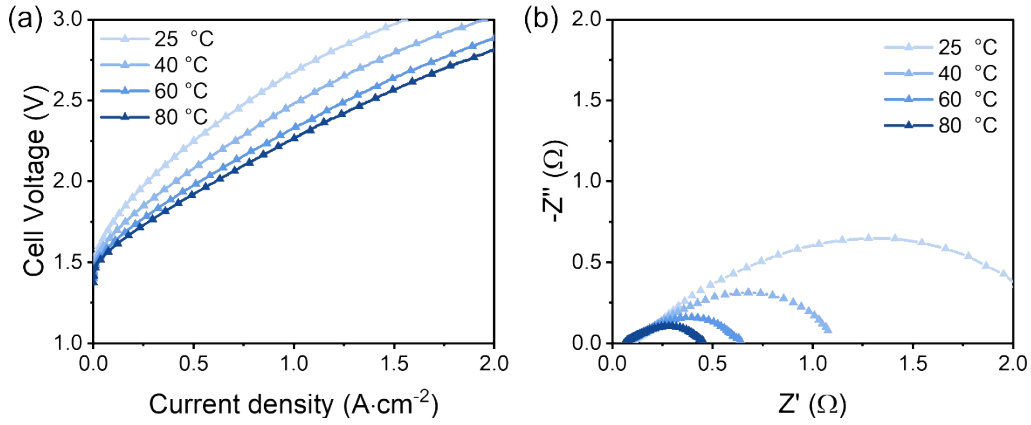

Fig. S21. (a) The Polarization curves and (b) the EIS Nyquist plots of the NiFe LDH-based AEMWE device under different temperatures.

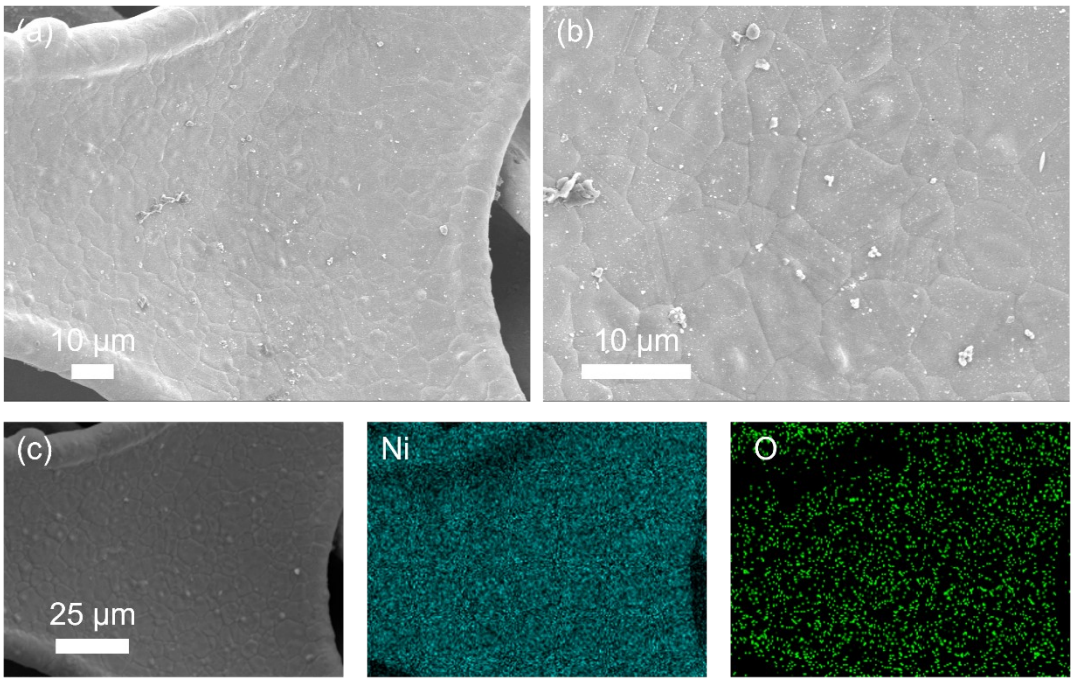

Fig. S22. (a,b) The SEM images of NiFe LDH after the CP test in AEMWE device under different magnifications and (c) the related EDS mappings of Ni and O elements.

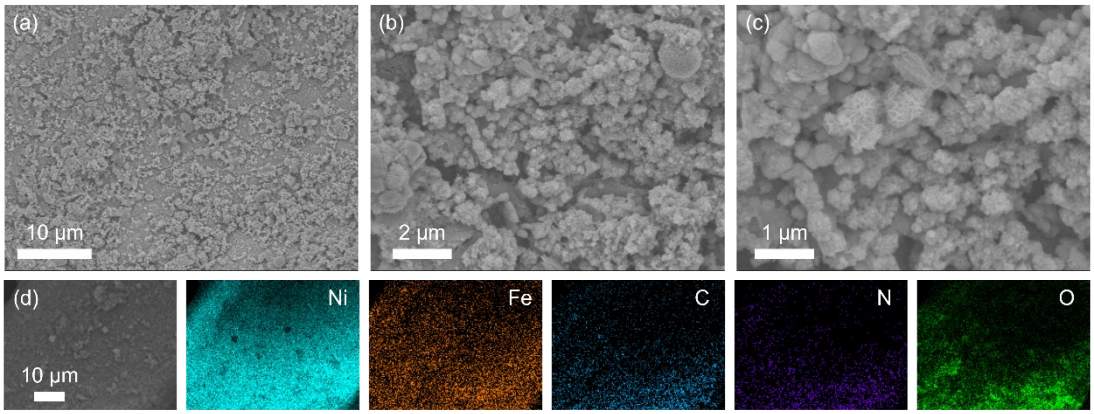

Fig. S23. (a-c) The SEM images of PANI/NiFe LDH after the CP test in AEMWE device under different magnifications and (c) the related EDS mappings of Ni, Fe, C, N and O elements.

After the CP test, the surface of NiFe LDH exhibited a smooth morphology characteristic of the NF substrate, and no Fe signal was detected in the EDS mapping, indicating that the catalyst structure had completely collapsed and leached away. In contrast, the PANI/NiFe LDH still retained its nanosheet morphology, with homogeneous distribution of Ni, Fe, C, N, and O signals in the EDS mapping. Compared with the three-electrode system, the flushing by liquids and bubbles in the anion exchange membrane water electrolyzer (AEMWE) device can generate strong mechanical stress, which tends to detach NiFe

LDH from the substrate. The PANI coating, however, helps mitigate such mechanical stress, thereby maintaining the stability of PANI/NiFe LDH.

Table S1. The ICP-OES results of Ni and Fe in PANI/NiFe LDH and NiFe LDH.

Samples	Ni Content ($\mu g \cdot cm^{-2}$)	Fe Content ($\mu g \cdot cm^{-2}$)	Molar ratio of Ni: Fe
NiFe LDH	174	51.1	3.24
PANI/NiFe LDH	167	50.8	3.13

Table S2. The ECSA calculated by the C_{dl} of electrodes in 1.0 $mol \cdot L^{-1}$ KOH.

Samples	ECSA (cm^2)
NiFe LDH	22.5
PANI	28.3
PANI/NiFe LDH	23.8

Table S3. The TOF of electrodes at 1.5 V vs. RHE in 1.0 $mol \cdot L^{-1}$ KOH.

Samples	TOF (s^{-1})
NiFe LDH	0.0552
PANI/NiFe LDH	0.0580

Table S4. The cell voltage of AEMWE devices based on NiFe LDH and PANI/NiFe LDH at 1.0 $A \cdot cm^{-2}$ and different temperatures.

AEMWE devices	25 °C	40 °C	60 °C	80 °C
NiFe LDH||Pt/C	2.67 V	2.48 V	2.33 V	2.26 V
PANI/NiFe LDH||Pt/C	2.55 V	2.41 V	2.26 V	2.13 V

Table S5. Comparison of the OER performance of PANI/NiFe LDH in this work and recently reported NiFe-based electrocatalysts.

Electrolyzer&Catalysts	Overpotential (mV)	Stability	Reference
PANI/NiFe LDH||Pt/C &PANI/NiFe LDH	**232@10 mA·cm^{-2} 275@100 mA·cm^{-2} 334@500 mA·cm^{-2}**	**200 h@500 mA·cm^{-2} (§) 500 h@500 mA·cm^{-2} (§§)**	**This work**
E-NiFe LDH||NFS	243@10 mA·cm^{-2}	22 h@10 mA·cm^{-2} (§)	Ref.[10]
Ru/d-NiFe LDH||Ru/d-NiFe LDH	220@10 mA·cm^{-2} 283@50 mA·cm^{-2}	140 h@100 mA·cm^{-2} (§)	Ref.[11]
60Fe/NF||NiMo	240@10 mA·cm^{-2} 304@100 mA·cm^{-2}	20 h@100 mA·cm^{-2} (§)	Ref.[12]
a/c-NiFe LDH||Pt/C	276@50 mA·cm^{-2} 297@100 mA·cm^{-2} 354@300 mA·cm^{-2}	130 h@1000 mA·cm^{-2} (§)	Ref.[13]
B_2-NiFe-(a-10) LDH||Pt mesh	290@100 mA·cm^{-2} 330@500 mA·cm^{-2}	40 h@1000 mA·cm^{-2} (§)	Ref.[14]
NiFe-P_{Zn}@PNTA	300@100 mA·cm^{-2}	360 h@100 mA·cm^{-2} (§§)	Ref.[15]
FeNi-LDH/MOF	263@100 mA·cm^{-2}	24 h@10 mA·cm^{-2} (§§)	Ref.[16]
FeB_i@FeNi LDH	243@10 mA·cm^{-2} 295@100 mA·cm^{-2}	90 h@100 mA·cm^{-2} (§§)	Ref.[17]
Cr-NiFe LDH	340@10 mA·cm^{-2}	6 h@10 mA·cm^{-2} (§§)	Ref.[18]
Cr-Ni_3S_2@Fe_xS_y/NIF	236@10 mA·cm^{-2}	100 h@150 mA·cm^{-2} (§§)	Ref.[19]

Note: § and §§ represent the test environment of the water electrolyzer and three-electrode system, respectively.

3 References

1. B. Ravel and M. Newville, *J. Synchrotron Radiat.*, 2005, **12**, 537-541.
2. S. Lee, L. Bai and X. Hu, *Angew. Chem.*, 2020, **132**, 8149-8154.
3. M. W. Louie and A. T. Bell, *J. Am. Chem. Soc.*, 2013, **135**, 12329-12337.
4. I. Harada, Y. Furukawa and F. Ueda, *Synth. Met.*, 1989, **29**, 303-312.
5. Z. Morávková and E. Dmitrieva, *J. Raman Spectrosc.*, 2017, **48**, 1229-1234.
6. B. J. Waghmode, S. H. Patil, M. M. Jahagirdar, V. S. Patil, R. P. Waichal, D. D. Malkhede, S. D. Sathaye and K. R. Patil, *Colloid. Polym. Sci.*, 2014, **292**, 1079-1089.
7. Y. Lin, H. Wang, C. K. Peng, L. Bu, C. L. Chiang, K. Tian, Y. Zhao, J. Zhao, Y. G. Lin, J. M. Lee and L. Gao, *Small*, 2020, **16**, e2002426.
8. Z. Karami, M. Jouyandeh, J. A. Ali, M. R. Ganjali, M. Aghazadeh, S. M. R. Paran, G. Naderi, D. Puglia and M. R. Saeb, *Prog. Org. Coat.*, 2019, **136**, 105218.
9. L. Liu, Y. Chen, Q. Zhang, Z. Liu, K. Yue, Y. Cheng, D. Li, Z. Zhu, J. Li and Y. Wang, *Appl. Catal. B*, 2024, **354**, 124140.
10. B. Zhang, Y. Ji, D. Shi, S. Wang, P. Zhang, S. Zhang and F. Lu, *J. Electroanal. Chem.*, 2025, **981**, 118958.
11. Y. Chen, Y. Liu, W. Zhai, H. Liu, T. Sakthivel, S. Guo and Z. Dai, *Adv. Energy Mater.*, 2024, **14**, 2400059.
12. Y. Zhuo, D. Liu, L. Qiao, S. Chen, J. Lu, W. F. Ip, H. Pan and Z. Wang, *Adv. Energy Mater.*, 2023, **13**, 2301921.
13. H. Ye, J. Zhang, Q. Chen, C. Feng, Z. Quan, G. Zhang, X. Fan, J. Zhang and Y. Li, *J. Energy Chem.*, 2025, **111**, 650-658.
14. Y. Ma, J. Wang, X. Liu, N. Xu, X. Li, Y. Wang, L. Zhao, Y. Chai and B. Dong, *Chem. Eng. J.*, 2024, **490**, 151490.
15. Y. Zhou, N. Jin, Y. Ma, Y. Cui, L. Wang, Y. Kwon, W. K. Lee, W. Zhang, H. Ge and J. Zhang, *Adv. Mater.*, 2023, **35**, e2209500.
16. H. Qin, J. Cheng, P. Zhou, Z. Ji, H. Peng, X. Shen, H. Zhou, G. Zhu and J. Yang, *Chem. Eng. J.*, 2024, **493**, 152721.
17. F. Wang, B. Liu, H. Wang, Z. Lin, Y. Dong, N. Yu, R. Luan, Y. Chai and B. Dong, *J. Colloid Interface Sci.*, 2022, **610**, 173-181.
18. X. Liu, X. Fan, H. Huang, H. Lin and J. Gao, *J. Colloid Interface Sci.*, 2021, **587**, 385-392.
19. Y. Zhang, Y. Yang, B. Lu, R. Zhang, F. Zhou, D. Sun, Q. Wang, J. Li and Z. Lei, *Fuel*, 2025, **402**, 135909.